Optical Filters for Narrow Band Light Adaptation on Imaging Devices

Rodrigo Henrique Gounella, Talita Conte Granado, João Paulo Campos da Costa, *Student Member, IEEE*, and João Paulo Carmo

***Abstract*—The imagiology using Narrow Band Light (NBL) is widely employed in detection of mucosa's premature changes of gastrointestinal tract, while taking advantage of light spectral features by enhancing the vascular structures without the application of any type of dye. NBL uses two specific spectral bands centered in blue (415 nm) and green (540 nm). Despite their greater advantages, this technique is not available on intra-corporal imagiology devices yet. Thus, this paper presents a low-cost method to adapt such devices without the need to develop specific and expensive LEDs (Light-Emitting Diodes) centered at 415 nm and 540 nm. The method combines optical filters with commercial LEDs to provide transmitted light with the desired peaks at 415 nm and 540 nm. Two optical filters were designed and fabricated, using 7 thin-films layers of SiO_2 and TiO_2 deposited by RF sputtering. The measurements showed that the transmitted light through the filters presented relative transmittance peaks located at 414 nm and 542 nm wavelengths with relative transmittances of 31% and 62% and FWHM (Full-Width-Half-Maximum) of 17 nm and 29 nm, respectively. The measurements also showed significant relative transmittances located at NBL central wavelengths of 415 and 540 nm with 30% and 60%.**

***Index Terms*—Narrow Band Light (NBL), Intra-corporal Imagiology, Optical filters, Thin-films, RF sputtering, Optical measurements.**

I. Introduction

THE illumination with narrow band light (NBL) allows the visualization of lesions and other details not identified with white light with great potential for medical applications. Examples of medical application of the NBL technique include the higher [1], [2] endoscopy and lower endoscopy (colonoscopy) [3], [4]. The NBL takes advantage of light spectral features to enhance vascular structures without the application of any type of dye by using two specific spectral bands centered in blue (415 nm) and green (540 nm) [5], [6]. While the 415 nm enhances the superficial veins and other mucosa structures visualization, the 540 nm enhances the deeper structures visualization, such as the sub-epithelial capillaries. The studies about light interaction with biological tissues have proven that longer the wavelength, the deeper is the penetration in tissues [7]. Unfortunately, only a few small bowel portions are accessible with the conventional endoscopy. This result in the impossibility to detect the early stages of most common diseases (e.g., bleeding, ulcer, and tumors) and therefore, missing the opportunity to control their evolution [8]. This absence of diagnosis can result in their deterioration into cancer or in some other vital diseases [9]. This is the reason behind the rise of a new class of intra-corporal imagiology devices, e.g., the smart pills, which have constituted a breakthrough in the way that inner body images were acquired. This also explains why the smart pills have become a first-line procedure for examining the gastrointestinal tract hidden places (e.g., the small bowel) [10]. Despite the greater advantage, this technique is not available on any intra-corporal imagiology device yet. This paper presents a low-cost method to adapt these devices (even the smart pills currently available in the market) without the need to develop specific and expensive LEDs at 415 nm and 540 nm. The method combines low-cost optical filters with low-cost commercial LEDs in order to provide light centered at 415 nm and 540 nm. Two optical filters were designed and fabricated for 415 nm and 540 nm, using successive thin-films layers of silicon dioxide (SiO_2) and titanium dioxide (TiO_2).

Manuscript received February 21, 2020; revised October 5, 2020; accepted November 14, 2020. Date of publication November 19, 2020; date of current version December 3, 2020. This work was supported by CNPq Project 400110/2014-8. *(Corresponding author: Rodrigo Henrique Gounella).*

The authors are with the Department of Electrical Engineering, University of São Paulo, 13566590 São Carlos, SP, BRAZIL (e-mail: rodrigogounella@usp.br; talitaconteg@usp.br; joaoccosta@usp.br; jcarmo@sc.usp.br).

Color versions of one or more figures in this article are available at https://doi.org/10.1109/JSTQE.2020.3039164.

Digital Object Identifier 10.1109/JSTQE.2020.3039164

II. Concept and Design

A. General Concept, Materials and Followed Strategy

The intra-corporal imagiology device can be adapted, using two options. The first option uses customized LEDs, whose transmitting peaks can match the desired wavelengths. The second option uses commercial LEDs, following their adaptation with optical filters. It is technologically easier and cheaper the customized optical filters fabrication than customized LEDs fabrication. For this reason, it was selected the second option to provide the Narrow Band Light (NBL) adaptation to avoid their fully redesign.

Fig. 1 illustrates the general concept, where the objective is optical filters fabrication, which in conjunction with commercial blue and green LEDs will present relative transmittance peaks at 415 nm and 540 nm, respectively. It must be noted that depending of relative transmittance FWHM (Full-Width-Half-Maximum), the peaks are allowed to shift slightly from the 415 nm and 540 nm. The FWHM must ensure that at 415 nm and 540 nm the relative transmittance is at least 90% of those measured at the peaks location.

1077-260X © 2020 IEEE. Personal use is permitted, but republication/redistribution requires IEEE permission.
See https://www.ieee.org/publications/rights/index.html for more information.

Authorized licensed use limited to: UNIVERSIDADE DE SAO PAULO. Downloaded on April 19,2021 at 16:48:22 UTC from IEEE Xplore. Restrictions apply.

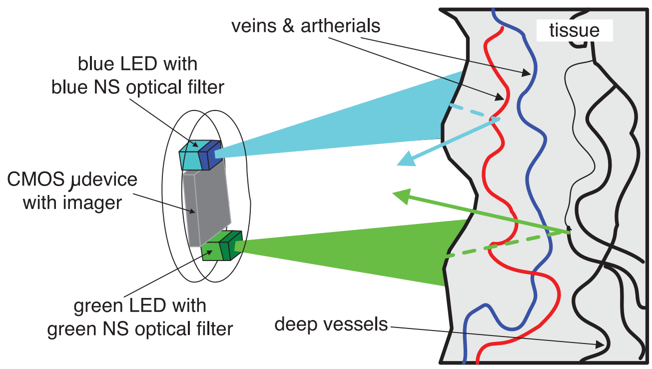

Fig. 1. General concept behind the adaptation of intra-corporal imagiology imagiology devices.

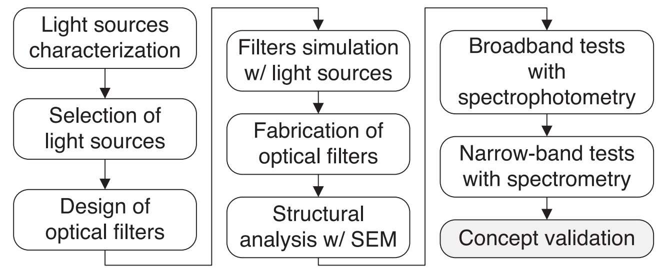

Fig. 2. A flowchart illustrating the workflow that was followed during the design, fabrication and structural/optical characterization of the filters.

Commercial filters are widely available at reasonable prices [11]–[13] and widely used on medical imaging [14]–[16]. These filters were the first option under consideration. However, this demands customized cuts to allow the placement and fixation of the filters above the respective small-sized LEDs. For this reason and to better and easily trim the passing wavelength in terms of relative transmittance, it was decided to fabricate the optical filters made of Fabry-Perot etalons. A Fabry-Perot etalon has a resonance cavity separated by two parallel and identical reflecting mirrors with a certain amount of transmittance through them, in order to create a strong resonance on a given wavelength [17]. This results on a cavity-thickness dependent wavelength resonance, given by:

$$l = 2q.n_{cavity}.d.\cos(\alpha) \quad (1)$$

where q is an integer number that gives the interference order, α is the light rays incidence angle with respect to the upper mirror, n_{cavity} is the refractive index inside the cavity and d [m] is the distance between the mirrors. Therefore, the materials must be selected in order to provide high (H) and low (L) refraction indexes in visible range. The silicon dioxide (SiO_2) and titanium dioxide (TiO_2) were selected as H and L materials because both can be obtained using physical processes, e.g., both can be deposited by sputtering, both are compatible in the sense that their mutual adhesion is high, and the silicon dioxide presents refraction index practically constant in the visible range [18], [19]. The sputtering also provides good characteristics for the films, including good control of the deposition rate [20], uniform film compliance [21], and flexibility in controlling films refractive indexes [22].

Fig. 2 shows the complete workflow of the followed strategy towards the design, fabrication and structural and optical characterization of the optical filters.

According to Fig. 2, the first step to follow was the characterization of the light sources available in the market as the most suitable candidates for selection (Sub-section II.B). Then, the optical filters were designed and simulated together with the selected light sources to obtain their relative transmittances (Sub-section II.C). Once the design was completed, the filters were fabricated (Sub-section III.A) and characterized to verify the specifications (Sub-section III.B).

B. Light Sources

The selected LEDs must be the smallest possible to allow their easy integration on small pills and at the same time, their spectral emission peaks must be located very close to the desired 415 nm and 540 nm wavelengths. Thus, for this reason it was selected the 0603 Surface Mount LED (SMD LED with 0603 footprint) from the Unique LEDs OEM to provide the blue illumination due to its typical transmitting wavelength between 400 nm and 410 nm, allowed supply voltages between 3.2 V and 3.8 V and with a 0603 footprint with a length of 1.6mm, a width of 0.8mm and an height of 0.6mm [23]. It was also selected the DualCom model K1893 with a 5730 footprint to provide the green illumination, due to its typical transmitting wavelength between 520 nm and 530 nm [24]. The selected LEDs spectral signature was acquired, using a Thorlabs portable spectrometer model CCS200. This spectrometer is controlled, using proprietary software running on a personal computer through a USB interface. This spectrometer can acquire spectrums within the whole visible range and more (e.g., bellow 400 nm in the ultraviolet range and above 750 nm in the infrared range), more specifically, between the 200 nm and 1000 nm. This spectrometer was also used to measure the normalized transmittances of the optical filters combined with the LEDs. Fig. 3 shows the spectral signature of both LEDs. The measurements made with the blue LEDs revealed a transmitting wavelength peak centered at 410 nm and a high relative transmittance of 65% at 415 nm, while the measurements made with the green LEDs revealed a peak centered at 533 nm and at the same time, providing a high relative transmittance of 88% at 540 nm.

C. Design Through Simulation

Each filter was designed for the minimum possible number of layers and at the same time to match the desired specifications in terms of peak location and FWHM smaller than 35 nm of the relative transmittances. It is important to have the smaller number of layers to facilitate the fabrication and decrease the fabrication costs. It is also important to have the same material to form the resonance cavity, but more important, the material with the smallest possible index of refraction that makes the resonance less sensitive to small variations in the thickness. The succession of materials and the thicknesses of the layers of both the top and bottom mirrors of the Fabry-Perot etalons are the same to facilitate their design and fabrication. For these

Authorized licensed use limited to: UNIVERSIDADE DE SAO PAULO. Downloaded on April 19,2021 at 16:48:22 UTC from IEEE Xplore. Restrictions apply.

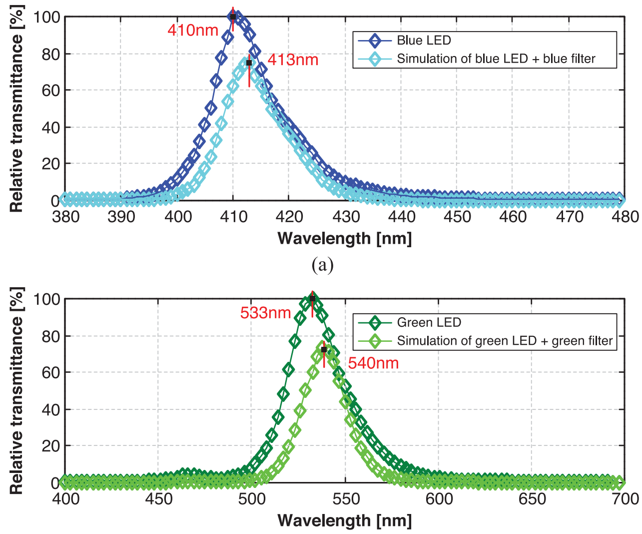

Fig. 3. Spectral signature and simulated relative transmittance considering the illuminants, e.g., the (a) blue and (b) green LEDs.

reasons, the optical filters are formed by a stack of seven layers, whose succession of refractive indexes follows the HLH-L-HLH structure. The thickness of each layer on the HLH structure ($th_{QW,i}$) is equal to a quarter of the guided wavelength ($\lambda_{g(i)}$) on that film:

$$th_{QW,i} = l_{g,i}/4 = l/(4n_i) \tag{2}$$

where n_i is the index of refraction of that layer (e.g., n_{L} and n_{H} for the L and H materials, respectively), while the thickness of the resonance cavity (th_{RC}) is equal to a half of the guided wavelength ($\lambda_{g\mathrm{L}}$):

$$th_{RC} = l_{g\mathrm{L}}/2 = 1\, l/(2n_{\mathrm{L}}) \tag{3}$$

where n_{L} is the index of refraction of that layer.

The design of optical filters must take into account the transmitting spectra of the selected light sources, thus, it was used the TFCalc software for such a purpose [25]. The design of blue and green filters took into account the wavelengths of 415 nm and 540m, respectively, in order to centralize the peak of relative transmittance. The design starts considering the theoretical thickness of each layer is given by the equations (2) and (3). Then, the thicknesses are adjusted by simulation to the desired relative transmittances, taking into account the spectral emission of each illuminant (e.g., of each LED). The equations (2) and (3) considered the indexes of refractions of 1.45 and 2.65 for the SiO_2 and for the TiO_2, respectively. The calculations done for the case of the blue filter centered at 514 nm with an ideal white illuminant resulted on approximately 71 nm for the SiO_2 and 39 nm for TiO_2 layers of the HLH structures and 143 nm for the resonance cavity. These same calculations done for the case of the green filter centered at 540 nm with an ideal white illuminant also resulted on approximately 93 nm for the SiO_2 and 51 nm for TiO_2 layers of the HLH structures and 186 nm for the resonance cavity. These values give a start-up

TABLE I
FILM THICKNESSES OF THE OPTICAL FILTERS OBTAINED BY SIMULATION

Layer #, index of refraction, material			Blue filter	Green filter
			Film thickness of each dielectric layer [nm]	
1	H	TiO_2	32	56
2	L	SiO_2	83	95
3	H	TiO_2	32	56
4 (cavity)	L	SiO_2	154	176
5	H	TiO_2	32	56
6	L	SiO_2	83	95
7	H	TiO_2	32	56

solution for the simulations, which must consider few realistic factors: the material of which the substrate of the filters is made, the incidence and transmission mediums, the thickness of the substrate, the characteristics of the detector and the incidence angle. In this sequence, the simulations took into account a 1mm-thick substrate made by the highly transparent glass B270 from the manufacturer Schott (with transmittance higher than 91.7%, index of refraction of 1.5229, dielectric constant of 7.5 and density of 2.56 g.cm^{-3}) [26] and combined with specific illuminant (blue [23] and green [24]). It was considered and ideal detector, air as the incidence and transmitting mediums, normal incidence and reference wavelengths of 415 nm and 540 nm [25]. The simulations were trimmed, using as starting points the theoretical values $th_{QW,i}$ and th_{RC} listed above and the seven thicknesses for both blue and green filters are presented in the Table I.

Fig. 3(a) and 3(b) shows the relative transmittances of both optical filters considering the layers obtained by simulations and respective blue and green LEDs spectral signatures. It is possible to observe from these figures a shift of the transmittance peaks from 410 nm to 413 nm and from 533 nm to 540 nm for blue and green illuminations cases, respectively, Moreover, it was stated by the simulations that the transmittances at 415 nm and 540 nm remained high, e.g., at more than 73%.

III. EXPERIMENTAL

Two preparatory procedures are required before fabricating the optical filters, more specifically, the substrates cleaning, where the filter will be fabricated on top, and the characterization of thin-films to adjust the thicknesses of layers to meet the filter's specifications. The optical filters fabrication and their optical and structural characterization follow just before the concept validation.

A. *Preparatory Procedures*

The cleaning procedure is necessary before doing the deposition of any thin-film to prevent the presence of particles and any kind of dirt within the deposition chamber and at the same time, to ensure that any impurity (grease and/or ions) is absent on top of the substrate surface. It was used a basic physical cleaning procedure rather than the Radio Corporation of America (RCA) cleaning procedure [27] to prevent the etching of the glass substrates with the latter. The former cleaning procedure follows

Authorized licensed use limited to: UNIVERSIDADE DE SAO PAULO. Downloaded on April 19,2021 at 16:48:22 UTC from IEEE Xplore. Restrictions apply.

a sequence of four steps. In the first step, the substrates are rinsed to remove grease from their surfaces. The substrates are kept immersed in detergent during three minutes. In the second step, the substrates are subjected to an ultrasonic bath of acetone during ten minutes. The third step also takes ten minutes with the samples being subjected to an ultrasonic bath of isopropanol. Finally, in the fourth and last step, the samples are rinsed in free of ions water during three minutes and then dried with nitrogen.

The second procedure consists in the thin-film deposition with the individual materials to adjust the deposition settings and at the same time, to get their optical properties to trim the thickness of the individual layers in the optical filter with relation to the values obtained by simulations (e.g., under ideal conditions). This procedure is crucial to have optical filters meeting as better as possible the targeted specifications. The thin-films of SiO_2 were deposited by PECVD (*Plasma-Enhanced Chemical Vapor Deposition*), while the thin-films of TiO_2 were deposited by DC sputtering, due to practical contingencies and equipment availability.

The DC sputtering depositions optimal settings to achieve TiO_2 films with the targeted refraction indexes resulted on argon and oxygen fluxes of 65 sccm and 40 sccm, respectively, while the power of the source was settled to 1 kW and the deposition chamber pressure was kept 20 mTorr (26.7×10^{-6} bar). These films were deposited at a rate of approximately 4.9 nm/min, while the refraction index presented a variation between 2.522 and 2.650 for 700 nm and 405 nm, respectively, e.g., very close to those observed in the literature [28]. The optical properties of the films made by TiO_2 were characterized using a Rudolph Auto EL III Ellipsometer EQP-00470 in the LSI, São Paulo - SP, Brazil. This ellipsometer only measure the refraction indexes for 405 nm, 630 nm and 830 nm wavelengths, requiring interpolation on other wavelengths for the simulations.

The PECVD depositions of SiO_2 were done at the pressure of 2 Torr (2.67×10^{-3} bar). The plasma was formed inside a reaction chamber with a grounded electrode and another electrode energized by a RF signal with a power of 40 W. The grounded electrode was used to keep the substrate in place and to subject it to a temperature of 400 °C. The reactant gases flux was settled to the best values to achieve the correct stoichiometry of SiO_2, otherwise, the films refraction index is higher than the targeted value if the ratio of Si:O is higher than 1:2. Thus and after a significant number of depositions, the best settings to the targeted refraction index were achieved with the reactant gases flux on 1000 sccm to N_2 and N_2O case and on 5sccm to SiH_4 case. These films were deposited at a rate of approximately 80 nm/min, while the refraction index presented a variation between 1.462 and 1.475. This variation on refraction index values was very close to those observed in the literature [29], [30]. The optical properties of the films made by SiO_2 were characterized using an Ellipsometer available in the CCS-Nano, UNICAMP, Campinas - SP, Brazil, because the former was out-of-the-order after the deposition of films made by SiO_2. It was only possible to measure the refraction index at 630 nm with this ellipsometer, and for this reason the settings were optimized for this wavelength.

TABLE II
FILM THICKNESSES OF THE FABRICATED AND SIMULATED BLUE FILTER

Layer #, index of refraction, material			Fabricated filter	Simulated filter
			Film thickness of each dielectric layer [nm]	
1	H	TiO_2	31.818	32
2	L	SiO_2	84.091	83
3	H	TiO_2	31.899	32
4 (cavity)	L	SiO_2	156.81	154
5	H	TiO_2	32.144	32
6	L	SiO_2	84.091	83
7	H	TiO_2	31.899	32

TABLE III
FILM THICKNESSES OF THE FABRICATED AND SIMULATED GREEN FILTER

Layer #, index of refraction, material			Fabricated filter	Simulated filter
			Film thickness of each dielectric layer [nm]	
1	H	TiO_2	56.467	56
2	L	SiO_2	94.111	95
3	H	TiO_2	56.488	56
4 (cavity)	L	SiO_2	177.250	176
5	H	TiO_2	56.488	56
6	L	SiO_2	94.124	95
7	H	TiO_2	56.488	56

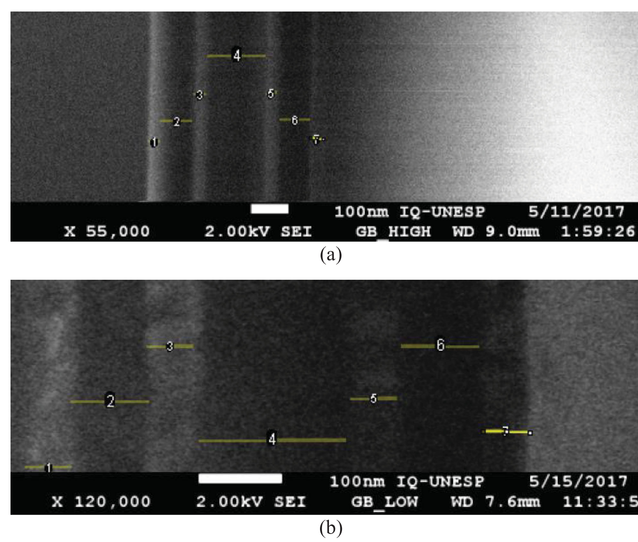

Fig. 4. SEM photographs showing the cross-sections of the fabricated (a) blue and (b) green filters.

B. *Filters Fabrication and Structural Characterization*

Table II presents the fabricated blue filter seven layers thicknesses and the comparison with theoretical targeted values by simulation for better visualization of the deposition processes quality. Table III reproduces the same results, but for the green filter. Fig. 4(a) and 4(b) shows SEM photographs in cross-section of the fabricated blue and green filters, respectively. The SEM photographs on Fig. 4 were acquired with a Field Emission Scanning Electron Microscope JEOL model JSM-7500F, operating at 2 kV (SEI) with the working distance (WD) set as 9 mm.

Authorized licensed use limited to: UNIVERSIDADE DE SAO PAULO. Downloaded on April 19,2021 at 16:48:22 UTC from IEEE Xplore. Restrictions apply.

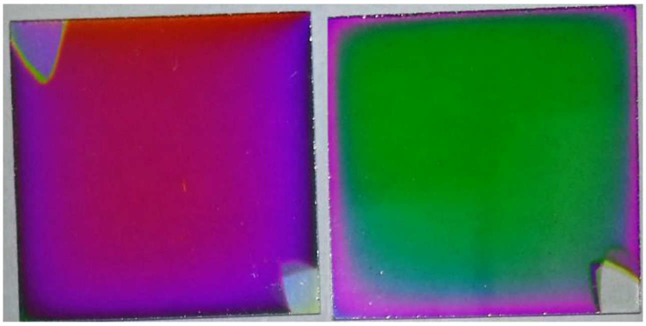

Fig. 5. Photographs of the fabricated blue and green filters.

As observed in Fig. 4 and complemented by the Tables II and III, the depositions presented a low deviation in relation to the targeted value, e.g., less than 2 nm on all depositions. Moreover, it is possible to clearly identify in Fig. 4 the separation between the seven layers with very low interface mixing (brighter layers correspond to TiO_2). Fig. 4 also reveals a good parallelism and flatness of the film's surface along the cross-section. This last issue is of major importance and a special care must be taking into account during the design and fabrication because the mirrors parallelism strongly affects the NBL filters internal cavity resonance and very sensible to the stray-light [31].

C. Optical Characterization

Fig. 5 shows photographs of selected samples of the fabricated (on left) blue and (on right) green filters. It is possible to observe a good fabrication quality in terms of uniformity measured on a wide range relative to the central region. The deposition pattern observed in the borders is not as uniform as in the central region of the sample. This phenomenon occurs because the angle of the deposition beam in the borders is higher than in the central location, resulting on a total thickness smaller in the former location. It is expected a shift in the transmittance peaks in the borders due to the thinning of the total thickness on this location.

Broadband tests with spectrophotometry and narrow-band tests with spectrometry were done in order to confirm the specifications in terms of the optical filters transmittances.

Figs. 6(a) and 6(b) show the photographs of the setups used to perform the spectrophotometry broadband tests and spectrometry narrow-band tests, respectively.

The broadband tests were the first set to be done to obtain the confirmation that the fabrication met the filters optical specifications. In this sequence, Figs. 7(a) and 7(b) present the transmittance measurement for the blue and green filter, respectively. A xenon lamp was used on these experiments to obtain the filters responses to this light source. Fig. 7(a) shows the response for the blue filter, where it is possible to observe a pass-band behavior centered at the ≈420 nm wavelength. However, it is also possible to observe that the response comprises the 415 nm wavelength with high transmittance of ≈51%. It is also possible to observe that the measurement made on the filter border revealed that the peak has shifted into the 433 nm. The explanation for this

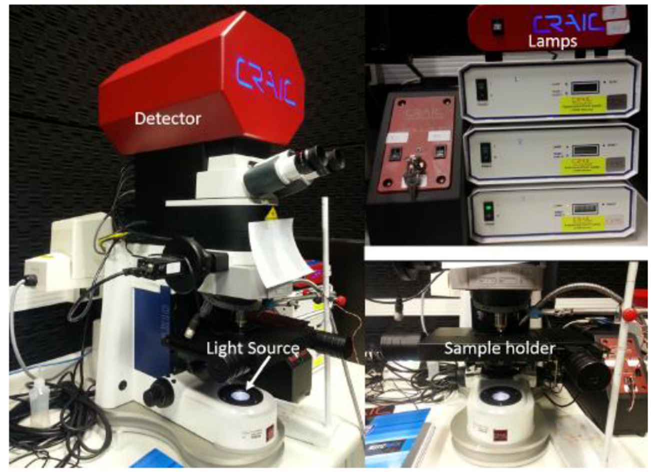

(a)

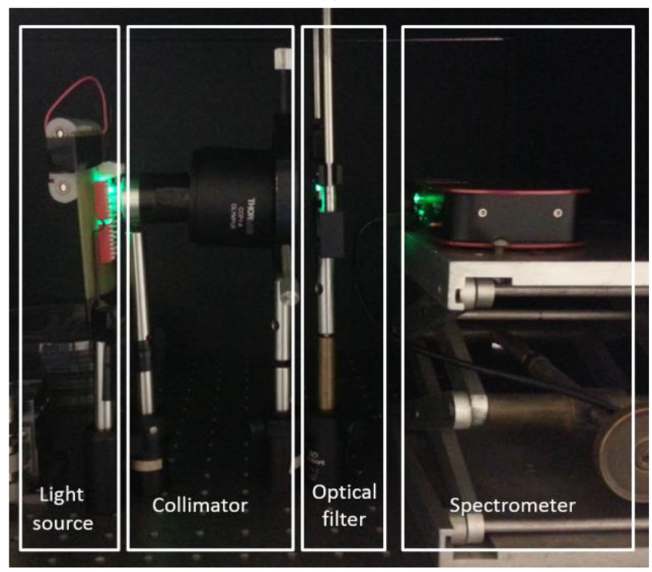

(b)

Fig. 6. Photograph of the experimental setup used to perform (a) the broadband characterization by spectroscopy, where it is possible to observe the sample holder (on right), three lamps (on right), the light source (on left) and the detector (on left); and (b) the narrow-band characterization by spectrometry, where it is possible to observe the components by looking from left into the right light, e.g., the light source, collimator, optical filter and the spectrometer.

occurrence is due to the deposition pattern at the border, which is not as uniform as in the samples middle. This results on a less thickness that desired.

Fig. 7(b) shows the green filter response with the xenon lamp used as the light source, where it is possible to observe a peak well located at 540 nm for the plot measured in the middle of the filter. It can also be observed fringes located at ≈400 nm with this light source. The measurements at border of the filter reveal a peak at 546 nm in result to a slight shift into the right. These results showed that even with broad-band xenon light incidence, the filter presents the desired wavelength peak at 540 nm.

The broadband measurement acted as a starting point for the narrow-band measurements execution, because it was expected a larger bandwidth than those of bandwidths working of the filters. The measurements during the broadband characterization

Authorized licensed use limited to: UNIVERSIDADE DE SAO PAULO. Downloaded on April 19,2021 at 16:48:22 UTC from IEEE Xplore. Restrictions apply.

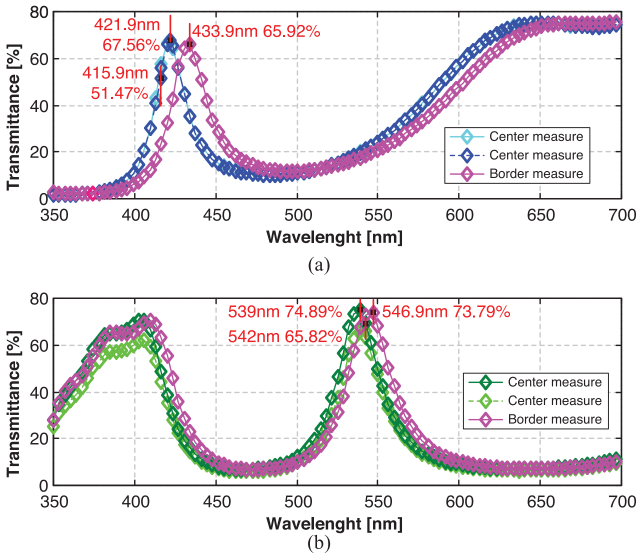

Fig. 7. Measured transmittance with a Xenon light for the (a) blue and (b) green filters. It can be observed in (b) a difference in the location of both center measures, because the measurement window is very narrow, so any slight difference or interference (like dust) can vary the result.

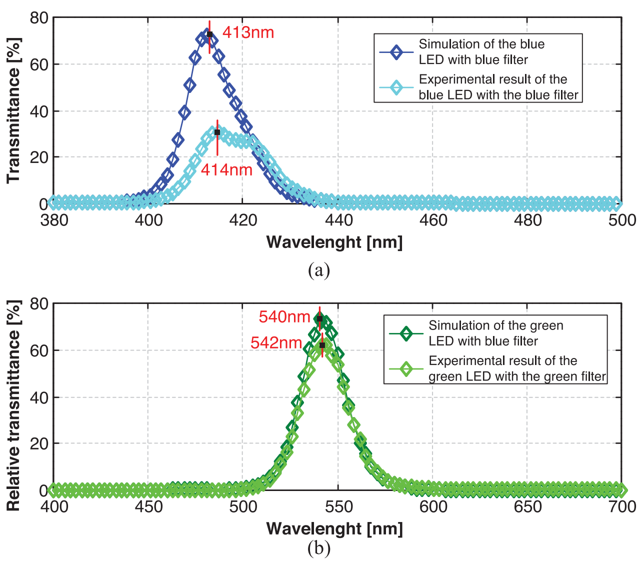

Fig. 8. Measurement results showing the relative transmittance of the (a) blue filter with a blue LED used as illuminant and the (b) green filter with a green LED used as illuminant.

showed the best results in the samples middle, meaning that the transmittance spectrums measured at these points have comprised both the wavelengths of interest (e.g., the 415 nm and the 540 nm). The conclusion to take before doing the narrow-band measurements is that the best expected results would be those made on these points (e.g., in the middle of the samples).

Fig. 8(a) shows the blue filter relative transmittance with the selected blue LED used as illuminant, while the Fig. 8(b) shows the green filter relative transmittance with selected green LED used as illuminant. It is possible to observe in Fig. 8(a) a relative transmittance with a peak value of 31% located at 414 nm, which is a good result when compared with the simulations.

TABLE IV
COMPARISON OF THE OPTICAL RESULTS WITH THE SIMULATIONS FOR BOTH FILTERS

414 nm	**Peak wavelength [nm]**	**FWHM [nm]**	**Maximum relative transmittance [%]**
Simulations	413	12	74
Experim.	414	17	31
Remarks	Can provide the 415 nm with $\lambda_{transmitted} \in [409,426]$ nm		
540 nm	**Peak wavelength [nm]**	**FWHM [nm]**	**Maximum relative transmittance [%]**
Simulations	540	27	73
Experim.	542	29	62
Remarks	Can provides the 540 nm with $\lambda_{transmitted} \in [528,557]$ nm		

The measurement results in the Fig. 8(a) are the blue filter relative transmission. In this sequence, it was already expected a relative transmittance smaller than the one obtained by simulation for the 415 nm wavelength due to the narrow spectral signature of the illuminant (blue LED). The fabrication issues also contributed to this difference. It must be noted that slight differences in the layers thicknesses affect more the optical filters transmittance characteristics centered in blue wavelengths than the ones centered in green wavelengths. The measurement results showed a slight deviation of 1 nm of the peak from the targeted 415 nm. The measurement results also showed a FWHM of 17 nm.

Fig. 8(b) shows the green filter measurement results. These measurements showed a relative transmittance peak of 62% located at 542 nm, presenting a FWHM of 29 nm. The peak was deviated 2 nm from the targeted 540 nm. Fortunately, the deviations are very small of both targeted wavelengths, which is not a severe impairment on NBL visualization either with green or with blue.

Table IV summarizes the main results and at the same time, makes a comparison with the simulations. This table confirms the feasibility to fabricate optical filters, which combined with blue and green light will match the specifications, e.g., peaks of the relative transmissions centered at 414 nm and 540 nm.

D. Concept Validation

After the realization of a first set of unsuccessful tests, it was realized have contaminated the photographs. Therefore, two lighting systems were fabricated, in order to enhance the illuminated area, and also to enhance the images quality. In this sequence, the new question that arise is where to place the optical filters, e.g., in the light source or in the imager?

It was taken the decision to make the test on the ocular mucosa of the glaucoma-blinded eye of the chief-coordinator of this research to validate the adaptation and to determine the optical filters best position. It is possible to observe in the photograph of the Fig. 9(a) the existence of a corneal ulcer clearly visible, which is the validation test target. Fig. 9(b1) and 9(b2) show the tests made with blue and green illumination, respectively, onto the ocular mucosa, with the filters (1) positioned on the

Authorized licensed use limited to: UNIVERSIDADE DE SAO PAULO. Downloaded on April 19,2021 at 16:48:22 UTC from IEEE Xplore. Restrictions apply.

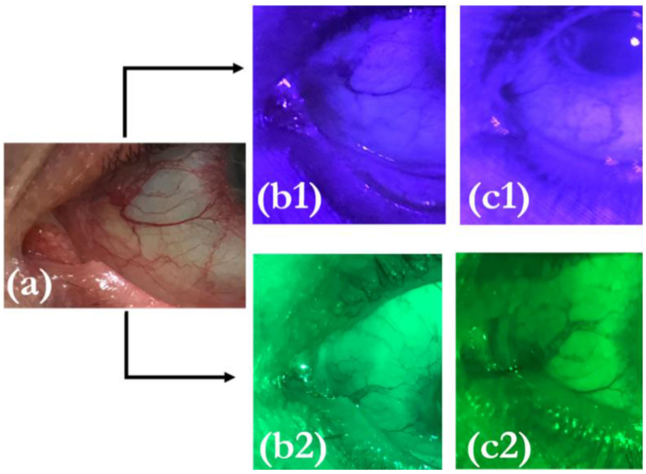

Fig. 9. Tests of the optical filter onto the ocular mucosa of the blind eye of the chief-coordinator of this research. (a) Reference picture taken under ambient light. The photos on (b1) and (b2) show the tests made with blue and green illumination, respectively, onto the ocular mucosa, with the filters positioned on the light sources. The photos on (c1) and (c2) show the tests made with blue and green illumination, respectively, onto the ocular mucosa, with the filters positioned on the image sensor.

light sources. For this system, the positioning of the optical filters on top of the LEDs showed great contrast enhancement and focus of the superficial vessels with the blue illumination. Fig. 9(c1) and 9(c2) show the tests made with blue and green illumination, respectively, onto the ocular mucosa, with the filters (2) positioned on the image sensor. The optical filters positioning on top of the image sensor showed a less focused image, but still with contrast enhancement of the superficial and deep vessels.

In resume, it was found that better images were obtained (regarding contrast enhancement and focus) with the optical filters positioned on top of the light sources. Thankfully and as expected, this validates the general concept on Fig. 1.

IV. Conclusion

Previous researches with Narrow Band Illumination (NBI) applied on intra-corporal imagiology devices have shown great advance when coupled with conventional endoscopy for the detections of lesions in the gastrointestinal tract. Thus, it is believed that the incorporation of the NBL into smart pills will be a great upgrade in the diagnosis, in the sense of detecting lesions non-visible with white light that most endoscopes have, in areas that the endoscopes cannot reach.

Acknowledgment

The authors would like to thank the CCS-Nano at University of Campinas (UNICAMP) with the deposition of thin-films. The authors also would like to thank the CDMF (FAPESP CEPID 2013/07296-2) at Federal University of São Carlos for the acquisition of SEM images.

References

[1] I. Rahman and P. Patel, “Impact of GI anatomic vectors on magnetic-assisted capsule endoscopy in the upper GI tract,” *Gastrointestinal Endoscopy*, vol. 89, no. 4, pp. 899–900, 2019.
[2] T. Krill *et al.*, “Outcomes of delayed endoscopic management for esophageal soft food impactions,” *Gastrointestinal Endoscopy*, vol. 91, no. 4, pp. 806–812, Dec. 2019.
[3] J. L. Garcia, S. Mão-de-Ferro, S. Faias, I. Marques, and A. D. Pereira, “Spontaneous colonic lipoma expulsion after diagnostic colonoscopy: A peculiar occurrence,” *Gastrointestinal Endoscopy*, vol. 91, no. 2, pp. 449-450, 2019.
[4] S. Thomas-Gibson and M. Matharoo, “Patient position change in colonoscopy: Dogmatic or pragmatic?,” *Gastrointestinal Endoscopy*, vol. 89, no. 6, pp. 1202–1203, 2019.
[5] K. Gono, “Multifunctional endoscopic imaging system for support of early cancer diagnosis,” *IEEE J. Sel. Top. Quantum Electron*, vol. 14, no. 1, pp. 62–69, Jan./Feb. 2008.
[6] Z.Y. Chen *et al.*, “Coherent narrow-band light source for miniature endoscopes,” *IEEE J. Sel. Top. Quantum Electron*, vol. 25, no. 1, 2019.
[7] M. F. Silva *et al.*, “NBI optical filters in minimally invasive medical devices,” *IEEE J. Sel. Top. Quantum Electron*, vol. 22, no. 4, Jul. Aug. 2016.
[8] G. Pan and L. Wang, “Swallowable wireless capsule endoscopy: Progress and technical challenges,” *Gastroenterol. Res. Pract.*, vol. 2012, Art. no. 841691.
[9] C. McCaffrey, O. Chevalerias, C. O’Mathuna, and K. Twomey, “Swallowable-capsule technology,” *IEEE Pervasive Comput.*, vol. 7, no. 1, pp. 23–29, 2008.
[10] M. Ibrahim and A. V. Gossum, “Novel imaging enhancements in capsule endoscopy,” *Gastroenterol. Res. Pract.*, vol. 2013, Art. no. 304723.
[11] Chroma technology corporation, single bandpass filters. [Online]. Available: https://www.chroma.com, 2020
[12] Semrock Inc., Individual Filters. [Online]. Available: https://www.semrock.com, 2020
[13] Thorlabs Inc., Spectral Filters. [Online]. Available: https://www.thorlabs.com, 2020
[14] Z. Nafar, R. Wen, and S. Jiao, “Visible light OCT-based quantitative imaging of lipofuscin in the retinal pigment epithelium with standard reference targets,” *Biomed. Opt. Express*, vol. 9, pp. 3768–3782, 2018.
[15] Z. Nafar, R. Wen, and S. Jiao, “Visible-light optical coherence tomography-based multimodal system for quantitative fundus autofluorescence imaging,” *Exp. Biol. Med.*, vol. 243, pp. 1265–1274.
[16] Z. Nafar, R. Wen, Z. Guan, Y. Li, and S. Jiao, “Quantifying lipofuscin in retinal pigment epithelium in vivo by visible-light optical coherence tomography-based multimodal imaging,” *Sci. Rep.*, vol. 10, 2020, pp. 1–10.
[17] G. Minas, J. S. Martins, J. C. Ribeiro, R. F. Wolffenbuttel, and J. H. Correia, “An array of fabry-perot optical-channels for biological fluids analysis,” *Sensors Actuators A*, vol. 115, 2004, pp. 362–367, 2004.
[18] G. Minas, J. C. Ribeiro, R. F. Wolffenbuttel, and J. H. Correia, “On-chip integrated CMOS optical detection microsystem for spectrophotometric analyses in biological microfluidic systems,” in *Proc. ISIE*, Dubrovnik, Croatia, 20-23 th, Jun. 2005, pp. 1133–1138.
[19] G. Minas, G. de Graff, R. F. WolffenButtel, and J. H. Correia, “An MCM-based microsystem for colorimetric detection of biomolecules in biological fluids,” *IEEE Sensors J.*, vol. 6, no. 4, pp. 1003–1009, Aug. 2006.
[20] G. Eisenstein and L. W. Stulz, “High quality antireflection coatings on laser facets by sputtered silicon nitride,” *Appl. Opt.*, vol. 23, no. 1, pp. 161–164, 1984.
[21] E. Baudet *et al.*, “Experimental design approach for deposition optimization of RF sputtered chalcogenide thin films devoted to enviro nmental optical sensors,” *Sci. Rep.*, vol. 7, 2017, Art. no. 3500.
[22] D. S. Ferreira, J. Mirkovic, R. F. Wolffenbuttel, J. H. Correia, M. S. Feld, and G. Minas, “Narrow-band pass filter array for integrated opto-electronic spectroscopy detectors to assess esophageal tissue,” *Biomed. Opt. Express, OSA*, vol. 2, pp. 1703–1716, 2011.
[23] Unique-LEDs, 0603 Surface Mount Led – Purple. [Online]. Available: https://www.unique-leds.com/leds/smd-leds/0603-smd/0603-surface-mount-led-purple/, 2018
[24] DualCom, LED 5730 0.5W Verde 520-530 nm SMD K1893. [Online]. Available: https://www.dualshop.com.br/led-5730-05w-verde-150ma-smd, 2018.
[25] Software Spectra, TFCalc: Software for the Design and Manufacture of Optical Thin Film Coatings. [Online]. Available: http://www.sspectra.com

Authorized licensed use limited to: UNIVERSIDADE DE SAO PAULO. Downloaded on April 19,2021 at 16:48:22 UTC from IEEE Xplore. Restrictions apply.

[26] Schott, B270 i Ultra-White Glass: Product information. [Online]. Available: https://www.schott.com/advanced_optics/english/products/optical-materials/thin-glass/ultra-white-glass-b-270-i/ind ex.html

[27] W. Kern, "The evolution of silicon wafer cleaning technology," *J. Electrochemical Soc.*, vol. 137, pp. 1887–1892, Jun. 1990.

[28] T. Siefke *et al.*, "Materials pushing the application limits of wire grid polarizers further into the deep ultraviolet spectral range," *Adv. Opt. Materials*,, vol. 4, no. 11, pp. 1780–1786, 2016.

[29] L. Gao, F. Lemarchand, and M. Lequime, "Exploitation of multiple incidences spectrometric measurements for thin film reverse engineering," *Opt. Express*, vol. 20, no. 14, pp. 15734–15751, 2012.

[30] L. Gao, F. Lemarchand, and M. Lequime, "Refractive index determination of SIO2 layer in the UV/VIS/NIR range: Spectrophotometric reverse engineering on single and Bi-layer designs," *J. Eur. Opt. Soc. Rapid Pub.*, vol. 8, Jan. 2013, Art. no. 3010.

[31] J. P. Carmo, R. P. Rocha, M. Bartek, G. de Graaf, R. F. Wolffenbuttel, and J. H. Correia, "A review of visible-range fabryperot microspectrometers in silicon for the industry," *J. Opt. Lasers Technol.*, vol. 44, no. 7, pp. 2321–2320, Oct. 2012.

Rodrigo Henrique Gounella was born in São Carlos, SP, Brazil, in 1991. He is Graduated in physics engineering from UFSCar, in 2016 and Mechanical Technician with SENAI Antonio Adolpho Lobbe, 2007. He received the M.Sc. degree in 2018 and conducts the Doctorate degree, both in electrical engineering with the Group of Metamaterials, Microwaves and Optics telecommunications at the USP, São Carlos, Brazil, where he developed a system for photodynamic therapy. He is currently developing scientific research on optical microsystems for biomedical applications and on radiofrequency hollograms for the Ka band (27–40 GHz).

Talita Conte Granado received the M.Sc. degree in 2017 in electrical engineering from the University of São Paulo (USP) in São Carlos - SP, Brazil. She is working as Biomedical Engineer. During her graduation, she worked for a year on the development of a Multielectrode Array during the sandwich period in Germany.

João Paulo Campos da Costa (Student Member) was born in Brazil. He Graduated in electrical engineering from the University of Araraquara in 2015. He received the M.Sc. degree in electrical engineering from the University of São Paulo (USP) in São Carlos-SP, Brazil, in 2018. He is currently working toward the Ph.D. degree in electrical engineering with USP of São Carlos.

João Paulo Carmo was born in Maia, Portugal, in 1970. He is Professor with the University of São Paulo (USP) in São Carlos - SP, Brazil. He is involved in the research on micro/nano-technologies, solid-state integrated sensors, and microdevices for biomedical and industrial applications. Professor Carmo is also Vice-Director of the Group of Metamaterials, Microwaves and Optics (GMeta).

Authorized licensed use limited to: UNIVERSIDADE DE SAO PAULO. Downloaded on April 19,2021 at 16:48:22 UTC from IEEE Xplore. Restrictions apply.